PAPER

Check for updates

Ultrasensitive flower-like TiO$_2$/Ag substrate for SERS detection of pigments and melamine†

Weiye Yang, [abc] Quanhong Ou, [abc] Chenyan Li,[abc] Mingming Cheng,[abc] Weijun Li[abc] and Yingkai Liu*[abc]

TiO$_2$ flower like nanomaterials (FLNMs) are fabricated *via* a hydrothermal method and Ag nanoparticles (NPs) are deposited *via* electron beam evaporation. Several biological pigments (CV, R6G and RhB) are selected as target molecules to investigate their surface enhanced Raman scattering (SERS) property. The results demonstrate ultrasensitivity and high reproducibility. They reveal that the limit of detection (LOD) is 4.17×10^{-16} M and the enhancement factor (EF) is 2.87×10^{10} for CV, and the LOD is 5.01×10^{-16} M and 7.94×10^{-14} M for R6G and RhB, respectively. To assess the reproducibility on TiO$_2$/Ag FLNMs SERS substrates, they are tested with 1.0×10^{-13} M of CV, 1.0×10^{-13} M of R6G and 1.0×10^{-11} M of RhB, respectively. The relative standard deviations (RSD) are less than 12.93%, 13.52% and 11.74% for CV, R6G and RhB, respectively. In addition, we carry out melamine detection and the LOD is up to 7.41×10^{-10} M, which is over 1000 times lower than the severest standards in the world. Therefore, the obtained TiO$_2$ FLNMs have potential application in detecting illegal food additives.

1. Introduction

Surface enhanced Raman scattering (SERS) has become an ultrasensitive and attractive spectroscopic technology in recent decades, which has generated great attention due to its nondestructive testing properties and high sensitivity. Generally, it is employed in the bioscience and medical fields, and analytical chemistry.[1–3] In actual application, SERS substrates are critical for detecting chemical molecules, not only high SERS performance, but also low cost and better reproducibility is demanded for a convenient SERS substrate.[4] Furthermore, as a general analysis technique, the operation should be simpler. Traditional substrates are focused on precious metals such as Au and Ag with morphologies of nanoparticles (NPs), nanocubes, nanorods, nanostars and core–shell NPs.[5,6] Due to their high cost, the semiconductor SERS substrates[7] have attracted significant attention, such as TiO$_2$, ZnO, CdS, CuO, SiO$_2$ and ZnS, *etc.*[8–14]

TiO$_2$ is a typical semiconductor material. It has been applied to environmental protection and solar energy due to its photocatalytic performance, chemical ability, and non-toxic

property.[15] Among these applications, TiO$_2$ nanoparticles (NPs) have been reported as active SERS substrates. The enhancement produced by TiO$_2$ NPs has been ascribed to charge-transfer mechanisms such as TiO$_2$-to-molecule and molecule-to-TiO$_2$ transfers.[16] In particular, Ag is considered to be one of the most excellent candidates for SERS application due to its highly plasmonic properties. Ag NPs not only supply surface plasmon resonance, but also interact with the incident laser to form electrons and holes between the substrate and the precious metal to enhance SERS performance. It is a high-efficiency strategy to deposit Ag NPs on the surface of TiO$_2$ for the generation of electrons and holes. Therefore, it is clearly that TiO$_2$ decorated by Ag NPs would be an excellent candidate for SERS substrate.[17]

Pigments, as crystal violet (CV), Rhodamine 6G (R6G) and Rhodamine B (RhB) are stable organic contaminants which have been widely used in various textile, pharmaceutical industries and aquacultures. Unfortunately, the inevitable pollution that discharged into drinking water are mutagenic and toxigenic/teratogenic towards living organisms, which can give rise to the increasing morbidities of tumor and cancer growth in bacteria, fishes, and mammalian cells.[18] Melamine is a triazine nitrogen organic compound and is deliberately mingled in milk and dairy drinks, which poses a major threat to food safety.[19] There are various methods to detect pigments and melamine, such as high performance liquid chromatography (HPLC),[20] liquid chromatography tandem mass spectrometry (LC-MS/MS),[21] gas chromatography.[22] However, these traditional techniques are either complicated or low detection efficiency, high skill for operators. Compared with traditional

ᵃYunnan Key Laboratory of Opto-Electronic Information Technology, Yunnan Normal University, Kunming 650500, China

ᵇCollege of Physics and Electronic Information, Yunnan Normal University, Kunming 650500, China

ᶜKey Laboratory of Advanced Technique & Preparation for Renewable Energy Materials, Ministry of Education, Yunnan Normal University, Kunming 650500, China. E-mail: liuyingkai99@163.com

† Electronic supplementary information (ESI) available. See DOI: 10.1039/d1ra08128d

methods, SERS technologies establish a simpler operation, convenient, and high sensitive technology in the future.

In this work, a newly SERS substrate is composed of TiO_2 flower like nanomaterials (FLNMs) and Ag NPs, TiO_2 FLNMs are prepared *via* a hydrothermal method and Ag NPs are deposited *via* the electron beam evaporation. It is used to detect pigment (CV, R6G and RhB) and melamine. This proposed SERS substrates achieve ultrasensitivity and high reproducibility. The results show that the proposed SERS method has a great potential for detection of illegal food additives with ultralow concentrations.

2.   Methods and experimental section

2.1   Reagents and instruments

Ti films (99.999% purity) are purchased from Haiyuan Aluminum Corporation, hydrofluoric acid (HF, 40 wt%) is supplied by Tianjin feng chuan chemical reagent Corporation, crystal violet (CV), Rhodamine 6G (R6G) and Rhodamine B (RhB) are supplied by Sinopharm Chemical Reagent Corporation, melamine is purchased from Maklin Corporation. All experimental water is deionized water with the resistance of 18.2 MΩ. All reagents are analytical grade and used as received.

The sample morphology is characterized by scanning electron microscope (SEM, Quanta FEG 250, FEI, USA) and its microstructure is further explored by transmission electron microscopy (TEM, JEOL 2010, Japan). X-ray diffraction (XRD, Ultima IV Rigaku, Japan) is used to verify phase of substrates. X-ray photoelectron spectroscopy (XPS, Thermo fisher Scientific, USA) is performed to reveal chemical valence states and chemical composition. The SERS signal is acquired from a confocal Raman spectrometer (Andor, England).

2.2   Preparation of TiO_2 FLNMs

TiO_2 FLNMs are prepared by a hydrothermal reaction between Ti film and HF solution according to the previous work.[23] The preparation of TiO_2/Ag FLNMs is followed our previous studies.[24]

The mainly process is as follows: firstly, Ti films (3 cm × 1 cm) are treated by a basic procedure of decontamination. Then, Ti films and 10 mmol HF 60 mL are transferred into a 100 mL Teflon autoclave, maintaining at the temperature of 110 °C for 6 h. After that, Ti films are rinsed with deionized water. Finally, TiO_2 films are dried at 80 °C and the resultant sample is obtained. The general reaction equations are as follows.

$$Ti + 6HF \rightarrow H_2TiF_6 + 2H_2\uparrow \tag{1}$$

$$H_2TiF_6 + 4H_2O \rightarrow Ti(OH)_4 + 6HF \tag{2}$$

$$Ti(OH)_4 \rightarrow TiO_2 + 2H_2O \tag{3}$$
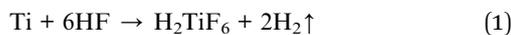
2.3   Preparation of TiO_2/Ag FLNMs

Ag NPs are deposited on the surface of TiO_2 FLNMs by electron beam evaporation. Evaporation rate is 0.1 Å s^{-1} and the thickness of Ag NPs is 6 nm (Fig. S1†). Thus, we obtain TiO_2/Ag FLNMs.

2.4   SERS measurement

Generally, the probe molecules are dropped on a substrate and then dry before SERS detection. Moreover, the coffee ring during the drying make the probe molecules uniformly distribute, led to poor reproducibility.[25,26] To alleviate this drawback, improving the detection efficiency and the uniformity of Raman signal, SERS test is examined in aqueous solution. First, TiO_2/Ag FLNMs films are immersed in the prepared solution for 3 h to achieve adsorption equilibrium. Then SERS substrate is put into a home-made quartz slot (15 mm × 15 mm × 1 mm) containing the corresponding solution covered with the cover glass. The SERS measurements are carried out with a confocal microscopy Raman spectrometer system. During SERS examination, the excitation laser is 532 nm. A 50× microscope objective is selected and 1200 (L mm^{-1}) grating is used. The acquisition time is 10 s and the accumulation number is three.

3.   Results and discussion

3.1   Structure and morphology

The morphology is firstly characterized by scanning electron microscope (SEM), SEM images of TiO_2 FLNMs are displayed in Fig. 1(a and b). Obviously, it shows that TiO_2 comprise abundant flower-like aggregates and have almost the same morphology. The size of TiO_2 FLNMs are around 0.9–1.7 μm (Fig. 1(e)). Fig. 1(c and d) portray SEM images of TiO_2/Ag FLNMs covered with Ag NPs with diameter of about 20–60 nm (Fig. 1(f)).

To further investigate structure of TiO_2/Ag FLNMs, The microstructures are analyzed by Transmission Electron
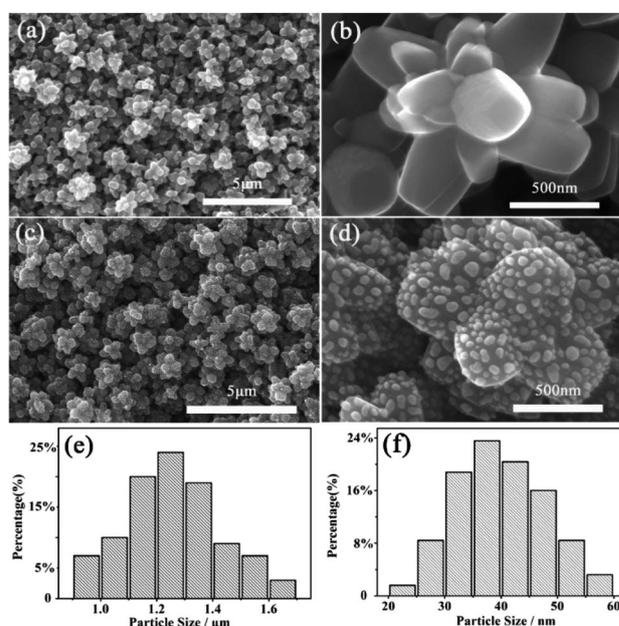

Fig. 1 SEM images of the samples. (a and b) TiO_2 FLNMs at low and high magnifications, respectively; (c and d) TiO_2/Ag FLNMs at low and high magnifications, respectively. (e and f) Particle size distribution histograms of TiO_2 FLNMs and Ag NPs, respectively.
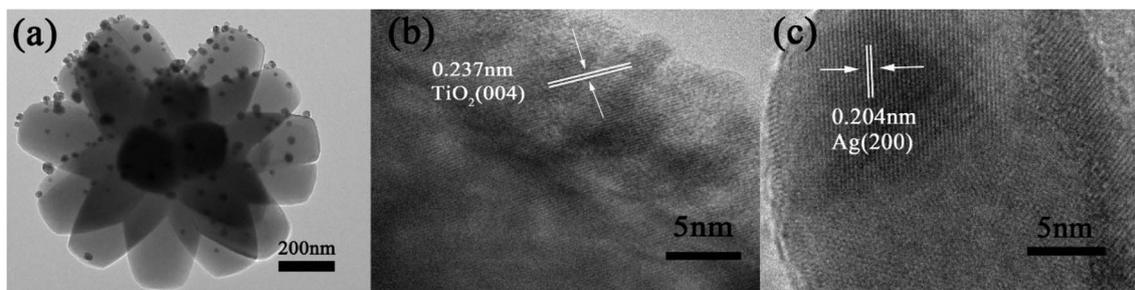
Fig. 2 TEM and HRTEM images of TiO$_2$/Ag FLNMs. (a) TEM images; (b) HRTEM of TiO$_2$; (c) HRTEM of Ag NP.

Microscope (TEM) (Fig. 2(a)). It reveals that the surface of the flower like TiO$_2$ material is covered with Ag NPs. Fig. 2(b) is a high-resolution TEM (HRTEM) images of TiO$_2$ FLNMs. The lattice fringes between nearby planes is 0.237 nm, corresponding to the (004) plane of anatase TiO$_2$. Fig. 2(c) is HRTEM image of the Ag NPs. The fringe spacing is 0.204 nm, matched with the (200) plane of the cubic Ag. From SEM images and TEM images, TiO$_2$/Ag FLNMs are formed.

The crystal phase structure of TiO$_2$ FLNMs and TiO$_2$/Ag FLNMs are further demonstrated by X-ray diffraction (XRD). Test conditions: X-ray source is a Cu-Kα1 target ($\lambda = 1.5406$ Å), the scanning angle range of 2θ was 10–80°, the voltage was 40 kV, the current is 35 mA, the step size was 0.02°, and the scanning speed is 0.25 s. All diffraction peaks in Fig. 3 are indexed to tetragonal structure TiO$_2$ with lattice parameters of $a = 3.785$ Å, $b = 3.785$ Å, $c = 9.514$ Å (JCPDS No. 21-1272). The diffraction peaks are sharp, indicating high crystalline.

The diffraction angles 2θ located at 25.28°, 37.80°, 48.05°, 53.89°, 55.06°, 62.88°, 68.76°, 70.31° and 75.03° are ascribed to the (101), (004), (200), (105), (211), (204), (116), (220) and (215) planes of anatase TiO$_2$. The blue curve belongs to the TiO$_2$/Ag FLNMs. No diffraction peaks of Ag are observed, probably because the ultrathin of deposited Ag film and low content.

3.2 XPS spectrum

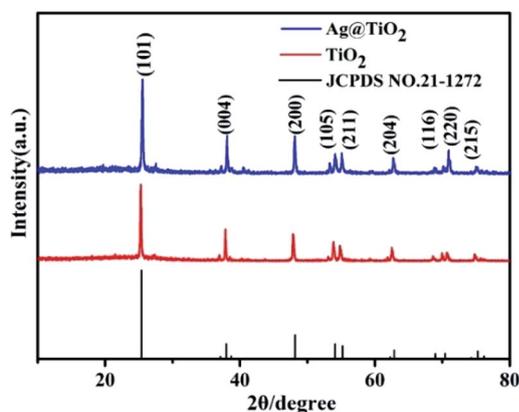X-ray photoelectron spectroscopy (XPS) is employed to analyze the elemental composition and chemical states of TiO$_2$/Ag FLNMs, as denoted in Fig. 4. In order to acquire accurate binding energy, the C 1s at 284.5 eV is utilized as the calibration. Fig. 4(a) displays the full scan XPS spectrum. It indicates that TiO$_2$/Ag FLNMs include Ti, O, C, F and Ag elements. F element originates from the residual of HF through the hydrothermal reaction. The peak at 684.1 eV belongs to F$^-$ absorbed on the surface of TiO$_2$.[27] Fig. 4(b) reveals the XPS bands for Ti 2p region. The peaks at 458.6 and 464.3 eV are assigned to Ti 2p$_{3/2}$ and Ti 2p$_{1/2}$, respectively, suggesting the presence of Ti^{4+} ions.[28] Fig. 4(c) is XPS band of O 1s. The characteristic peak of O 1s is included of two peaks fitted by Gaussian equation (Avantage, Thermo Fisher Scientific, USA). The peak located at 530. 8 eV comes from the O–Ti bonding, and the peak at 532.8 eV is ascribed to O$_2$ adsorption. XPS band of Ag 3d is shown in Fig. 4(d). The peaks at 367.3 and 373.3 eV are belonged to Ag 3d$_{5/2}$ and Ag 3d$_{3/2}$, respectively, revealing that Ag is deposited on the surface of the TiO$_2$ FLNMs.[29] These results demonstrate the successfully preparation of TiO$_2$/Ag FLNMs.

3.3 SERS applications

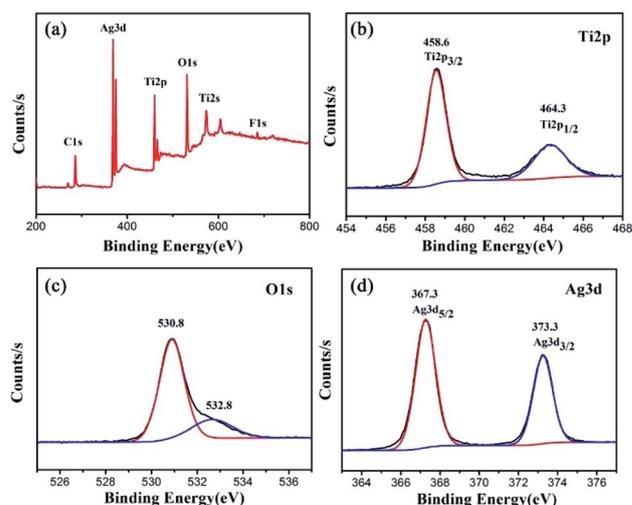Pigments (CV, R6G and RhB) have been worldwide applications and as a biological stain, fungicide in medicine, food

Fig. 3 XRD pattern of TiO$_2$ FLNMs and TiO$_2$/Ag FLNMs.

Fig. 4 XPS analyzation of TiO$_2$/Ag FLNMs. (a) Survey scan; (b) Ti 2p; (c) O 1 s; (d) Ag 3d.

additives and aquaculture. However, it is a strong carcinogen and clastogene. On the other hand, melamine is a cheap and easily accessible organic compound which is commonly used for dairy drinks throughout the world. These drugs recently have been restricted for use in the European Union, the United States, China, and many other countries. Because of their low cost high efficiency and easy accessibility, they are still illegally used. Therefore, sensitive detection of pigments and melamine is very promising for health and safety applications.[30]

3.3.1 SERS detection of CV. In order to estimate SERS property of TiO$_2$ FLNMs, Ag NPs, TiO$_2$/Ag FLNMs substrates, CV is firstly chosen as target molecule. Fig. 5(a, c and e) exhibited SERS signals of CV molecule with different concentrations, corresponding to TiO$_2$ FLNMs, Ag NPs, TiO$_2$/Ag FLNMs, respectively. It is seen that TiO$_2$/Ag FLNMs have the best SERS achievement. The minimum detection concentration on TiO$_2$/Ag FLNMs reached 1.0×10^{-15} M. The limit of detection (LOD)[31] is another important parameter for SERS performance. The intensity of the peak at 1621 cm^{-1} *versus* logarithmic concentration of CV for TiO$_2$ FLNMs, Ag NP and TiO$_2$/Ag FLNMs substrates are illustrated in Fig. 5(b, d and f). Its corresponding LODs are 7.76×10^{-6}, 7.08×10^{-10}, and 4.17×10^{-16} M, respectively.

The representative peaks of CV molecules with different concentrations are displayed in Fig. 5(e). The peak at 915 cm^{-1} is assigned to ring skeletal vibrational mode.[32] The peak at 1179 cm^{-1} rooted from C–H plane bending mode[33] and the band at 1374 cm^{-1} is attributed to C–N stretching mode.[34] The other peaks at 1590, 1621 cm^{-1} are the C–C stretching modes[35] and the band at 1120 cm^{-1} originates from the C–H out of plane bending vibration.[36] All peaks are consistent with the characteristic peaks of CV.

The enhancement factor (EF) is another critical parameter for SERS. In order to assess EF of TiO$_2$/Ag FLNMs, the peak at
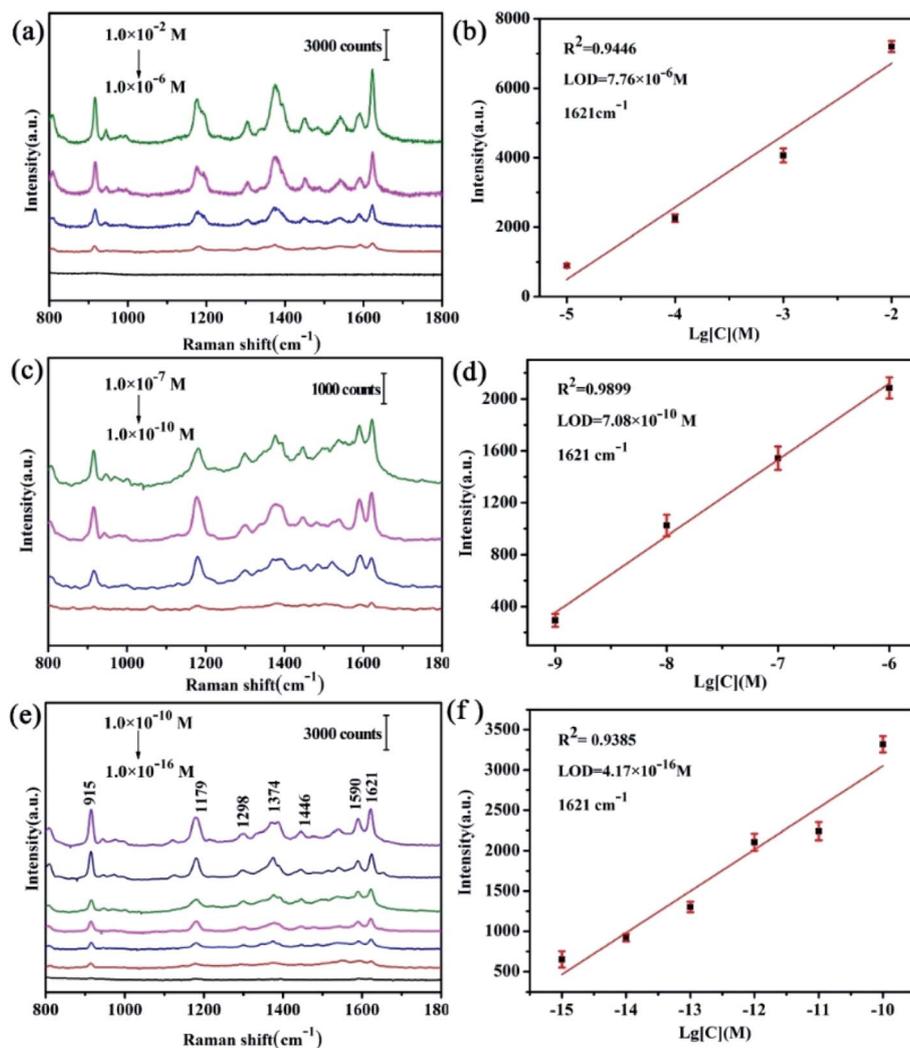

Fig. 5 Raman spectra of CV with various concentrations on TiO$_2$ FLNMs, Ag NPs, TiO$_2$/Ag FLNMs, respectively, (a) TiO$_2$ FLNMs; (b) the linear fit of the peak at 1621 cm^{-1} *versus* CV concentrations with TiO$_2$ FLNMs; (c) Ag NPs; (d) the linear fit of the peak at 1621 cm^{-1} *versus* CV concentrations with Ag NPs; (e) TiO$_2$/Ag FLNMs; (f) the linear fit of the peak at 1621 cm^{-1} *versus* CV concentrations with TiO$_2$/Ag FLNMs.

Fig. 7 (a) SERS signals with different concentrations of the melamine on the TiO$_2$/Ag FLNMs substrates; (b) the linear fit of the peak at 690 cm^{-1} *versus* melamine concentrations on the TiO$_2$/Ag FLNMs.

Table 1 LOD comparison of melamine on different substrates

SERS substrate	LOD (M)	Ref.
Ag NPs sandwich	10^{-9}	39
Bowl-like Au/Ag alloy	10^{-9}	42
Ag–Au hollow nanocubes	10^{-8}	43
Ag–Au microfluidic chip	10^{-8}	44
Ag–Au NDs	5.0×10^{-8}	48
Hydrogel micropellet	10^{-8}	49
TiO$_2$ FLNMs	7.41×10^{-10}	This work

shown in Fig. 7. The peak at 690 cm^{-1} is attributed to in plane deformation modes of triazine ring. Another weak peaks at 985 cm^{-1} is assigned to the δ(–CN).[40–42] All peaks belong to the characteristic peaks of melamine. In the meanwhile, it is worth noting that the strength of each Raman characteristic peak was related to concentration. It displays a linear relationship of $I = 27783.1 + 3017.5 \log[C]$ ($R^2 = 0.9479$) within the range of from 1.0×10^{-4} to 1.0×10^{-9} M. LOD is assessed to be 7.41×10^{-10} M in Fig. 7(b). Up to now, it is the lowest detection limit.[43–45] The limit of melamine in food is 2.5 ppm for non-infant formula products and 1 ppm for infant milk products[46] in China. The strictest standard in the world should be 0.15 ppm in liquid infant formulas proposed by the Codex Alimentarius Commission in 2012.[47] Therefore, LOD on the TiO$_2$/Ag FLNMs is over 1000 times lower than the severest standard in the world. Compared with other substrates, their LODs are listed in Table 1. It demonstrates that the proposed TiO$_2$/Ag
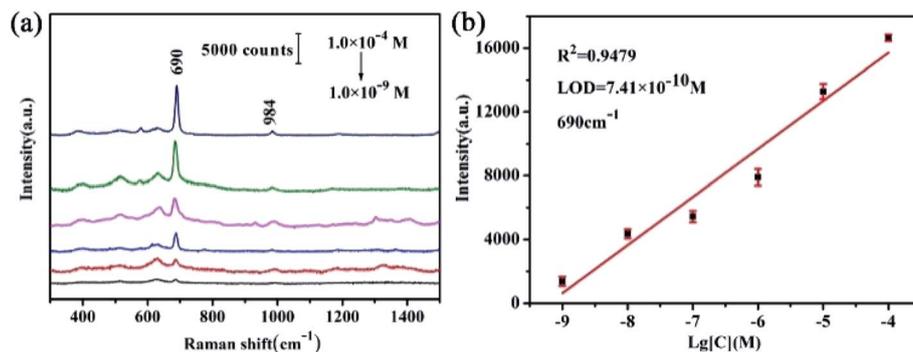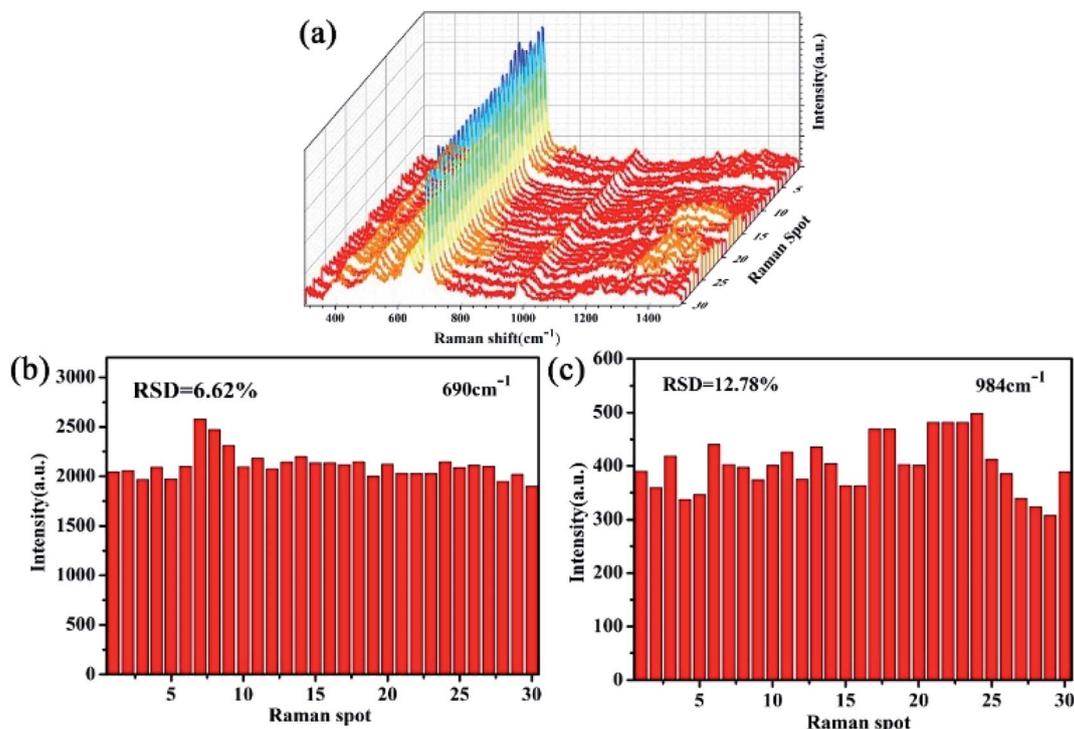

Fig. 8 (a) 3D Raman spectra of 10^{-7} M melamine molecules at 30 random spots on the TiO$_2$/Ag FLNMs; (b and c) RSDs of the selected peaks at 690 and 984 cm^{-1}, respectively.

FLNMs possess the lowest LOD. It can be extended to food safety monitoring.

To examine the reproducibility of SERS signals on TiO$_2$/Ag FLNMs, 3D SERS signals of melamine solution are acquired from 30 random spots with concentration of 1.0×10^{-7} M in Fig. 8(a). It reveals that prominent reproducibility is achieved, which is consistent with the SERS intensity at the characteristic peak.

The RSDs at peak 690 and 984 cm^{-1} are 6.62%, 12.78%, respectively (Fig. 8(b and c)). All the RSDs values are less than 12.78%, indicating TiO$_2$/Ag FLNMs substrates have high reproducibility.

3.4 Mechanism

SERS mechanism is usually governed by electromagnetic enhancement mechanism (EM) and charge-transfer mechanism (CT).[17,50] Compared with molecular adsorption, EM enhancement more depends on the structure of the substrate, being nonselective enhancement. Meanwhile, CT enhancement not only depends on the structure of the substrate but also on the molecular adsorption due to the electron transfer between substrate and molecule, improving the enhancement effect and exhibiting selective for the adsorbed molecules.[51,52] The reasons for TiO$_2$/Ag FLNMs' high SERS performance are as follows: firstly, as a principal factor, TiO$_2$ FLNMs have high uniform morphology for attaining remarkable SERS enhancement. Secondly, the surface-deposited Ag NPs supply high SERS enhancement effect in visible light region. Thirdly, with immersing procedure, the probe molecule adsorbed on the substrates completely, which is more avail to TiO$_2$-to-molecule charge transfer. The SERS enhancement of TiO$_2$/Ag FLNMs is synergetic contribution of the EM effect of Ag NPs and the CT effect of TiO$_2$-to-molecule, finite difference time domain (FDTD) simulations and the charge-transfer (CT) mechanism have been proved in our previous work.[24] As a result, it is reasonable that TiO$_2$/Ag FLNMs gain high SERS performance.

4. Conclusions

In this work, TiO$_2$/Ag FLNMs are synthesized by the hydrothermal reaction and electron beam evaporation. Pigments (CV, R6G, RhB) and melamine are employed for testing SERS performance and the corresponding LOD reach 4.17×10^{-16} M, 5.01×10^{-16} M, 7.94×10^{-14} M and 7.41×10^{-10} M, respectively. The LOD of melamine on the TiO$_2$/Ag FLNMs is over 1000 times lower than the most severe standards in the world. The RSD are less than 12.93%, 13.52%, 11.74% and 12.78% for CV, R6G, RhB and melamine, respectively. The high sensitivity and reproducibility demonstrate that the TiO$_2$/Ag FLNMs have a great potential application in food safety. It paves a new way for developing excellent performance SERS substrates.

Author contributions

Yingkai Liu guided the experiments and revised the paper; Quanhong Ou supplied help for SERS measurement; Mingming Cheng, Weijun Li and Chenyan Li supplied help for data analysis; Weiye Yang performed the design, fabrication a testing of the device, analyzed the data and wrote the paper. All authors have read and agreed to the published version of the manuscript.

Conflicts of interest

There are no conflicts to declare.

Acknowledgements

References

1 J. N. Anker, W. P. Hall, O. Lyandres, N. C. Shah, J. Zhao and R. P. Van Duyne, *Nat. Mater.*, 2008, **7**, 442–453.

2 J. Zheng, A. L. Jiao, R. H. Yang, H. M. Li, J. S. Li, M. L. Shi, C. Ma, Y. Jiang, L. Deng and W. H. Tan, *J. Am. Chem. Soc.*, 2012, **134**, 19957–19960.

3 C. X. Zhang, L. Su, Y. F. Chan, Z. L. Wu, Y. M. Zhao, H. J. Xu and X. M. Sun, *Nanotechnology*, 2013, **24**, 335501.

4 B. H. Zhang, H. S. Wang, L. H. Lu, K. L. Ai, G. Zhang and X. L. Cheng, *Adv. Funct. Mater.*, 2008, **18**, 2348–2355.

5 W. E. Smith, *Chem. Soc. Rev.*, 2008, **37**, 955–964.

6 I. Yoon, T. Kang, W. Choi, J. Kim, Y. Yoo, S. W. Joo, Q. H. Park, H. Ihee and B. Kim, *J. Am. Chem. Soc.*, 2009, **131**, 758–762.

7 A. Musumeci, D. Gosztola, T. Schiller, N. M. Dimitrijevic, V. Mujica, D. Martin and T. Rajh, *J. Am. Chem. Soc.*, 2009, **131**, 6040–6041.

8 C. W. Cheng, B. Yan, S. M. Wong, X. L. Li, W. W. Zhou, T. Yu, Z. X. Shen, H. Y. Yu and H. J. Fan, *ACS Appl. Mater. Interfaces*, 2010, **2**, 1824–1828.

9 C. Y. Li, C. X. Yang, W. J. Li, M. M. Cheng and Y. K. Liu, *Nano*, 2020, **15**, 2050122.

10 C. X. Yang, C. Qing, Q. J. Wang, X. J. Zhang, J. Lou and Y. K. Liu, *Sens. Actuators, B*, 2020, **304**, 127218.

11 N. D. Jayram, S. Sonia, P. S. Kumar, L. Marimuthu, Y. Masuda, D. Mangalaraj, N. Ponpandian, C. Viswanathan and S. Ramakrishna, *RSC Adv.*, 2015, **57**, 46229–46239.

12 N. D. Jayram, D. Aishwarya, S. Sonia, D. Mangalaraj, P. S. Kumar and G. M. Rao, *J. Colloid Interface Sci.*, 2016, **477**, 209–219.

13 R. Purbia, P. D. Nayak and S. Paria, *Nanoscale*, 2018, **27**, 12970–12974.

14 M. Ramuthai, S. Habibuddin, S. Sonia, N. D. Jayram, K. D. A. Kumar, M. Shkir, H. Algarni and S. Alfaify, *J. Mater. Sci.: Mater. Electron.*, 2021, **22**, 26596–26607.

15 S. F. Zhang, X. D. Yang, Y. H. Numata and L. Y. Han, *Energy Environ. Sci.*, 2013, **6**, 1443–1464.

16 A. I. López-Lorente, R. A. Picca, J. Izquierdo, C. Kranz, B. Mizaikoff, C. Di Franco, S. Cárdenas, N. Cioffi, G. Palazzo and A. Valentini, *Microchim. Acta*, 2018, **185**, 1–9.

17 H. Fang, C. X. Zhang, L. Liu, Y. M. Zhao and H. J. Xu, *Biosens. Bioelectron.*, 2015, **64**, 434–441.

18 Y. Tian, H. Zhang, L. L. Xu, M. Chen and F. Chen, *Opt. Lett.*, 2018, **43**, 635–638.

19 J. M. Zhang, S. C. Qu, L. S. Zhang, A. W. Tang and Z. G. Wang, *Spectrochim. Acta, Part A*, 2011, **79**, 625–630.

20 G. Venkatasami and J. R. John Jr, *Anal. Chim. Acta*, 2010, **665**, 227–230.

21 M. S. Filigenzi, B. Puschner, L. S. Aston and R. H. Poppenga, *J. Agric. Food Chem.*, 2008, **56**, 7593–7599.

22 B. Puschner, R. H. Poppenga, L. J. Lowenstine, M. S. Filigenzi and P. A. Pesavento, *J. Vet. Diagn. Invest.*, 2007, **19**, 616–624.

23 M. Liu, L. Y. Piao, W. M. Lu, S. T. Ju, L. Zhao, C. L. Zhou, H. L. Li and W. J. Wang, *Nanoscale*, 2010, **2**, 1115–1117.

24 W. Y. Yang, J. Q. Tang, Q. H. Ou, X. Q. Yan, L. Liu and Y. K. Liu, *ACS Omega*, 2021, **6**(41), 27271–27278.

25 E. Avci and M. Culha, *RSC Adv.*, 2013, **3**, 17829–17836.

26 X. Lin, W. L. J. Hasi, X. T. Lou, S. Lin, F. Yang, B. S. Jia, D. Y. Lin and Z. W. Lu, *RSC Adv.*, 2014, **4**, 51315–51320.

27 J. H. Pan, X. Zhang, A. J. Du, D. D. Sun and J. O. Leckie, *J. Am. Chem. Soc.*, 2008, **130**, 11256–11257.

28 C. Y. Jimmy, J. Y. Yu, W. K. Ho, Z. T. Jiang and L. Z. Zhang, *Chem. Mater.*, 2002, **14**, 3808–3816.

29 X. Y. Li, G. X. Zhu, L. S. Xiao, Y. J. Liu, Z. Y. Ji, X. P. Shen, L. R. Kong and S. A. Shah, *J. Alloys Compd.*, 2019, **773**, 40–49.

30 W. Ahmed, O. Demirtas, I. M. Ozturk and A. Bek, *ACS Appl. Nano Mater.*, 2020, **3**, 6766–6773.

31 D. Vernardou, M. Apostolopoulou, D. Louloudakis, N. Katsarakis and E. Koudoumas, *J. Colloid Interface Sci.*, 2014, **424**, 1–6.

32 Y. Yokota, K. Ueno and H. Misawa, *Small*, 2011, **7**, 252–258.

33 B. W. Yang, Z. M. Liu, Z. Y. Guo, W. Zhang, M. M. Wan, X. C. Qin and H. Q. Zhong, *Appl. Surf. Sci.*, 2014, **316**, 22–27.

34 J. J. Yu, M. Z. Shen, S. Y. Liu, F. Li, D. P. Sun and T. H. Wang, *Appl. Surf. Sci.*, 2017, **406**, 285–293.

35 Y. Z. Zhou, J. P. Huang, W. D. Shi, Y. Li, Y. Y. Wu, Q. Q. Liu, J. Zhu, N. Zhao, L. L. Zhang, J. Yang and X. N. Cheng, *Appl. Surf. Sci.*, 2018, **457**, 1000–1008.

36 J. Q. Tang, C. Y. Zeng, Y. Q. Wang, Z. W. Lin and S. Q. Man, *Plasmonics*, 2015, **10**, 563–568.

37 D. Shao, S. Bi, R. Zhao, X. Y. Sun, X. Li and J. F. Yu, *Sens. Actuators, B*, 2020, **307**, 127644.

38 K. K. Xu, *J. Opt.*, 2018, **20**, 024014.

39 J. M. Zhang, S. C. Qu, L. S. Zhang, A. W. Tang and Z. G. Wang, *Spectrochim. Acta, Part A*, 2011, **79**, 625–630.

40 Z. Kartal and A. Yavuz, *J. Mol. Struct.*, 2018, **1155**, 171–183.

41 D. Li, D. Y. Lv, Q. X. Zhu, H. Li, H. Chen, M. M. Wu, Y. F. Chai and F. Lu, *Food Chem.*, 2017, **224**, 382–389.

42 N. E. Mircescu, M. Oltean, C. Vasile and N. Leopold, *Vib. Spectrosc.*, 2012, **62**, 165–171.

43 B. Nie, B. Luo, J. Shi, L. Gao and G. T. Duan, *Sens. Actuators, B*, 2019, **301**, 127087.

44 J. M. Li, Y. Yang and D. Qin, *J. Mater. Chem. C*, 2014, **2**, 9934–9940.

45 R. Wang, Y. Xu, R. J. Wang, C. Y. Wang, H. Z. Zhao, X. Q. Zheng, X. Liao and L. Cheng, *Microchim. Acta*, 2017, **184**, 279–287.

46 C. M. Gu, T. Lan, H. C. Shi and Y. Lu, *Anal. Chem.*, 2015, **87**, 7676–7682.

47 H. Y. Zou, K. L. Xu, Y. Y. Feng and B. Liang, *Food Anal. Methods*, 2015, **8**, 740–748.

48 Y. Sun, X. D. Zhai, Y. W. Xu, C. Liu, X. B. Zou, Z. H. Li, J. Y. Shi and X. W. Huang, *Food Control*, 2021, **122**, 107772.

49 D. Sun, F. H. Cao, H. M. Wang, S. L. Guan, A. L. Su, W. Q. Xu and S. P. Xu, *Sens. Actuators, B*, 2021, **327**, 128943.

50 A. Otto, *J. Raman Spectrosc.*, 2005, **36**, 497–509.

51 X. Jiang, Y. L. Chen, J. Du, X. L. Li, Y. Shen, M. Yang, X. X. Han, L. B. Yang and B. Zhao, *J. Raman Spectrosc.*, 2018, **49**, 1257–1264.

52 Y. Zhou, J. Chen, L. Zhang and L. B. Yang, *Eur. J. Inorg. Chem.*, 2012, **19**, 3176–3182.